STATISTICS, OPTIMIZATION AND INFORMATION COMPUTING
Stat., Optim. Inf. Comput., Vol. **16**, Month 2026, pp 0–14.
Published online in International Academic Press (www.IAPress.org)

Design of a State Feedback Controller for the Stabilization of a Magnetic Levitation System Considering a Nonlinear Second-Order Dynamic Model

Carlos Andrés Vergara-Espitia, Johan Sebastián Sánchez-Rodríguez, Oscar Danilo Montoya*

Facultad de Ingeniería, Universidad Distrital Francisco José de Caldas, Bogotá D.C. 110121, Colombia

Abstract This paper addresses stabilization and reference tracking in a magnetic levitation system, characterized by its inherent nonlinearity and open-loop instability. A second-order dynamic model of the system is derived, considering the injected current as the control input. An exact linearization procedure based on error dynamics is employed to obtain an equivalent linear representation. From this model, two state-feedback control strategies are developed: a conventional approach and an extended formulation incorporating integral action to ensure the accurate tracking of the reference position. The performance of the proposed schemes is evaluated against a decoupled nonlinear proportional–integral controller using metrics related to stability, transient response, and control effort. The results demonstrate the structural advantages of the state-space-based approach, highlighting its systematic capability to meet dynamic specifications while improving closed-loop behavior under disturbances and parametric variations.

Keywords Magnetic levitation system, state-feedback controller, second-order dynamic model, linear control

DOI: 10.19139/soic-2310-5070-3747

1. Introduction

Throughout history, humans have developed tools with the aim of expanding their capabilities and optimizing their daily activities. From the earliest mechanical instruments to today's automated systems, technological evolution has been closely linked to the need to improve efficiency, reduce physical effort, and increase precision in performing different tasks [1]. As civilization advances, these tools have ceased to be mere mechanical extensions and become increasingly complex systems, integrating electrical, electronic, and computational components capable of operating under variable and dynamic conditions, such as lifting heavy loads, cutting, and transporting materials [2]. Even in the 21st century, there remains a keen interest in refining the processes that still require human intervention. This is why many industrial and technological processes currently depend on the ability of these systems to maintain stability and performance in the face of external disturbances and internal uncertainties [3].

As technological systems have become increasingly complex, so too have the demands placed on them in terms of precision, stability, and adaptability. Many modern devices operate under dynamic conditions, where small variations in internal variables can have a significant impact on the overall behavior [4]. This sensitivity has driven the development of increasingly rigorous analysis methodologies, aimed not only at describing the system but also at ensuring its safe and efficient operation across different scenarios. In this regard, the study of dynamic systems with nonlinear and unstable characteristics has become an area of particular interest in the field of control engineering [5].

Thus, mathematical modeling takes on central importance, as it allows representing these phenomena by means of differential equations that describe their internal variables. This is essential for understanding and predicting the dynamics of complex physical systems [6], where only the input and output parameters are typically known.

*Correspondence to: O. D. Montoya (Email: odmontoyag@udistrital.edu.co). Facultad de Ingeniería, Universidad Distrital Francisco José de Caldas, Bogotá D.C. 110121, Colombia.

ISSN 2310-5070 (online) ISSN 2311-004X (print)

Magnetic levitation is a field of great interest in control engineering, given the nonlinear and inherently unstable nature of its dynamics [7]. Designing an efficient controller requires a precise understanding of system dynamics [8]. However, when developing its mathematical model, several levels of uncertainty inevitably arise, given the high complexity of representing all the disturbances and variations that affect its behavior [4]. These characteristics position magnetic levitators as a suitable platform for validating advanced control techniques [9], especially those aimed at coping with behaviors that are highly sensitive to disturbances and parametric variations.

The open-loop instability of the system implies that small deviations from the equilibrium point can lead to rapid divergence in the position of the mass [10], which requires control strategies that are capable of ensuring stability and dynamic performance under formal criteria. In many cases, traditional solutions rely on empirical tuning schemes or nonlinear proportional–integral controllers designed around specific operating conditions [11]. Although these approaches may be functional in particular scenarios, they do not always provide a systematic framework to guarantee transient response specifications, closed-loop pole placement, and robustness against model uncertainties [12].

Under these conditions, addressing the problem from a state-space representation enables a more complete description of the interaction between the electrical and mechanical variables of the system. This not only facilitates stability analysis around the reference point; it also provides an appropriate framework for designing control strategies with clearly defined performance criteria.

Over time, control theory has developed a wide variety of methodologies aimed at ensuring stability, dynamic performance, and robustness against disturbances. In general, these approaches can be grouped into two main categories: deterministic and heuristic strategies. The former are based on explicit mathematical models of the system and rigorous analytical tools. This category includes classical controllers such as proportional-integral (PID) [13] and state-feedback control. On the other hand, heuristic strategies rely on approaches inspired by biological processes or artificial intelligence techniques, *e.g.*, neural networks and fuzzy logic [14], which make it possible to address systems that are highly nonlinear or exhibit significant structural uncertainty.

Among the physical systems most commonly used to validate and compare these strategies, magnetic levitators stand out, particularly regarding the control of a metallic sphere immersed in a vertical magnetic field generated by an electromagnet. In this system, the position of the sphere is typically regulated using proportional–integral (PI) controllers that rely on measurements of the magnetic flux or the current in the coil as the feedback variable [15]. This system is especially attractive due to its inherently open-loop and unstable nature and its marked nonlinear behavior, making it an ideal platform for the comparative evaluation of different control approaches.

Under this premise, each author selects the strategy they consider most suitable to better control the state variables, optimize settling times, or minimize the steady-state error. Magnetic levitation systems have gained significant relevance in scientific research, not only for their educational value but also for their ability to represent nonlinear systems that are experimentally accessible and exhibit dynamics comparable to various industrial processes [16]. This characteristic positions them as intermediate testbeds between purely theoretical models and highly complex real-world applications.

The interest in these systems is also explained by their potential for technology transfer. The control principles developed in levitation platforms can be extrapolated to larger-scale applications, such as high-speed trains based on magnetic levitation [17,18], as well as to automated industrial processes in laboratory environments [19], packaging and handling systems, robotic platforms [20], and biomedical devices [21]. Furthermore, they are still widely used in academic experimentation to validate advanced control models and algorithms [22].

Among the most common deterministic strategies in this type of application is state-feedback control, which uses the system's state variables to directly influence its internal dynamics, enabling the placement of poles at desired locations and, consequently, the design of the system's transient response and the steady-state behavior [23]. When not all variables can be measured directly, one must to resort to the use of observers or state estimators [24], which introduces an additional stage in the design process but significantly expands the applicability of the method. In this context, the performance evaluation of these strategies is often complemented by control indices, which allow establishing quantitative criteria to identify the alternative with the best behavior [25]. Additionally, with the aim of bringing the analysis closer to more realistic operating conditions, disturbances in the form of noise can be incorporated into position measurement [26], thus enabling the evaluation of the system's robustness against this type of uncertainty.

This article proposes a control strategy based on the state-space approach for a magnetic levitation system, systematically addressing its nonlinear and inherently unstable dynamics. This approach ensures asymptotic stabilization around the equilibrium point, meeting performance criteria in both the transient and steady-state regimes. The effectiveness of our method is validated through a comparative analysis against strategies reported in the literature, considering different scenarios that include parametric variations and external disturbances. This analysis enables a quantitative evaluation of the robustness and overall performance of the controller. Additionally, as an extension of the study, a stage is incorporated which introduces noise into position measurement, in order to approximate the system's behavior to more realistic conditions and analyze the robustness of the controller in the presence of measurement uncertainties.

The remainder of this contribution is organized as follows. Section 2 presents a description of a magnetic levitation system (MLS), including its mathematical model. Section 3 details the implementation of the analyzed control strategies. Section 4 presents the results obtained, and, finally, Section 5 outlines the conclusions of this work along with future research directions.

2. Modeling the magnetic levitation system

This section introduces the mathematical model of the MLS under study, which is based on a third-order representation adapted from [27]. A state-space formulation is then used to describe the error dynamics in the vicinity of the equilibrium point. Figure 1 illustrates the schematic diagram of the MLS, where F_{mag} denotes the electromagnetic force generated by the current i circulating through the inductor L; F_{g} corresponds to the gravitational pull exerted on the ferromagnetic mass m; R stands for the internal resistance of the coil; v is the input voltage applied; and e represents the equivalent voltage measured via the Hall-effect sensor, as outlined in [27].

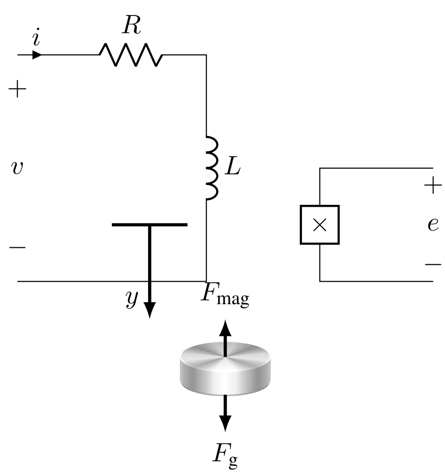

Figure 1. Schematic representation of a MLS [28]

The modeling procedure is structured as follows. Subsection 2.1 presents the nonlinear dynamic model of the system, Subsection 2.2 introduces the incremental model and defines the equilibrium point, Subsection 2.3 derives the exact feedback linearization, and Subsection 2.4 formulates the state-space representation of the system.

2.1. Nonlinear dynamic model

The model under study is an inherently unstable nonlinear system whose control objective is to regulate the vertical position of a metallic sphere through the force generated by an electromagnet, as described in Figure 1. By applying Newton's second law [29] to the vertical dynamics of the sphere, *i.e.*,

$$m\ddot{y} = F_g - F_{\text{mag}}, \tag{1}$$

where m is the mass of the sphere; y denotes its vertical position, measured from the electromagnet; $F_g = mg$ is the gravitational force; and F_{mag} is the electromagnetic force exerted by the current in the electromagnet. The latter is modeled as a nonlinear function of the current i and the position y, following the approach proposed in [30].

$$F_{\text{mag}} = k_{\text{mag}} \left(\frac{i}{y^3} \right), \tag{2}$$

where k_{mag} is a constant that characterizes the geometry and magnetic properties of the actuator. By substituting (2) into (1), the nonlinear dynamic model of the system is obtained:

$$\ddot{y} = g - \frac{k_{\text{mag}}}{m} \left(\frac{i}{y^3} \right), \tag{3}$$

2.2. Incremental model and equilibrium point

For the controller design, an operating point that corresponds to the desired equilibrium position $y^\star$ is defined. The following incremental state variables are introduced:

$$\eta = y - y^\star, \qquad \zeta = \dot{y}. \tag{4}$$

The control current is denoted as $\omega = i$. When (3) is expressed in terms of these variables, the dynamic model takes the form below:

$$\dot{\eta} = \zeta, \tag{5}$$

$$\dot{\zeta} = g - \frac{k_{\text{mag}}}{m} \left(\frac{\omega}{(\eta + y^\star)^3} \right), \tag{6}$$

At the equilibrium point, $\zeta^\star = 0$ is satisfied, and the steady-state current required to compensate for the gravitational action is as follows:

$$\omega^\star = \frac{mg}{k_{\text{mag}}} \left(y^\star \right)^3. \tag{7}$$

2.3. Exact linearization by feedback

Given the nonlinear nature of Equations (5) and (6), the input–output exact feedback linearization technique is applied in order to obtain an equivalent linear dynamic representation. To this effect, the following transformation of the control input is defined:

$$\omega = (\eta + y^\star)^3 \frac{m}{k_{\text{mag}}} (g - u), \tag{8}$$

where u is an auxiliary control signal to be designed. By substituting (8) into (6), the nonlinearities are algebraically canceled, and the decoupled second-order system is obtained:

$$\dot{\eta} = \zeta, \tag{9}$$

$$\dot{\zeta} = u. \tag{10}$$

This system corresponds to a double integrator, a canonical representation in control theory that enables the systematic design of linear control laws for the original nonlinear plant, following the state-space analysis framework presented in [31].

2.4. State space representation

The Linearized System (9)–(10) is expressed in the standard state-space form:

$$\dot{x} = Ax + Bu, \tag{11}$$

where the state vector and the system matrices are defined as follows:

$$x = \begin{bmatrix} \eta \\ \zeta \end{bmatrix}, \quad A = \begin{bmatrix} 0 & 1 \\ 0 & 0 \end{bmatrix}, \quad B = \begin{bmatrix} 0 \\ 1 \end{bmatrix}. \tag{12}$$

Note that the pair (A, B) defined in (12) is completely controllable, a necessary and sufficient condition for arbitrary pole placement through state feedback. This equivalent linear model is shared by the two control strategies presented in Section 3.

3. State feedback control strategies

Based on the linear state-space model obtained in Section 2, two state-feedback control strategies are designed to stabilize the MLS and ensure robust reference tracking. The first corresponds to standard state-feedback (SF) control [32], formulated to modify the system's dynamics through pole placement. This approach, detailed in Subsections 3.1.1 and 3.1.2, is suitable when the system model is accurate and no external disturbances are present. The second extends this strategy by incorporating integral action [33,34] with the aim of ensuring reference tracking in the steady state as well as the rejection of constant disturbances. This leads to the formulation of an augmented system model and the design of a state-feedback controller with integral action [35], which is developed in Subsections 3.2.1 through 3.2.3. Both controllers share the exact feedback linearization structure described in (8) and use Ackermann's formula [36] for pole placement.

3.1. State feedback control

3.1.1. Control law Based on the representation (11), the following state-feedback control law is proposed:

$$u = -Kx, \tag{13}$$

where $K = \begin{bmatrix} k_1 & k_2 \end{bmatrix}$ is the state-feedback gain vector, following the formulation presented in [32]. By substituting (13) into (11), the closed-loop dynamics are obtained:

$$\dot{x} = (A - BK)\, x. \tag{14}$$

The values of $(A - BK)$ completely determine the transient response of the system and can be placed at arbitrary locations in the complex plane through an appropriate selection of K.

3.1.2. Design by pole placement The Controller Gains (13) are calculated using Ackermann's formula [36]. The performance specifications are expressed in terms of the settling time T_s and the damping ratio ξ, from which the natural frequency is obtained:

$$\omega_n = \frac{4}{\xi\, T_s}. \tag{15}$$

The two desired closed-loop poles are selected as follows:

$$p_1 = -\omega_n, \qquad p_2 = -\alpha\, \omega_n, \tag{16}$$

with $\alpha > 1$ to avoid repeated poles and improve numerical robustness. The gains are obtained by evaluating

$$K = \texttt{acker}(A,\, B,\, [p_1,\, p_2]). \tag{17}$$

3.2. State feedback control with integral action

Although the SF controller ensures the asymptotic stability of the decoupled system, its performance may degrade in the presence of parametric uncertainties or step-type disturbances, situations in which steady-state error may arise. To eliminate this error, the architecture is extended by incorporating an integral state [33,34], thus giving rise to the controller.

3.2.1. Augmented system with integral action The integral state variable x_I is introduced, defined by the following dynamics:

$$\dot{x}_I = \eta, \tag{18}$$

which accumulates the position error over time. By incorporating (18) into Equations (9) and (10), the augmented system is obtained, following the approach presented in [35]:

$$\dot{\eta} = \zeta, \tag{19}$$

$$\dot{\zeta} = u, \tag{20}$$

$$\dot{x}_I = \eta, \tag{21}$$

whose matrix representation takes the standard form:

$$\dot{x}_a = A_a\, x_a + B_a\, u, \tag{22}$$

with

$$x_a = \begin{bmatrix} \eta \\ \zeta \\ x_I \end{bmatrix}, \quad A_a = \begin{bmatrix} 0 & 1 & 0 \\ 0 & 0 & 0 \\ 1 & 0 & 0 \end{bmatrix}, \quad B_a = \begin{bmatrix} 0 \\ 1 \\ 0 \end{bmatrix}. \tag{23}$$

The pair (A_a, B_a) is completely controllable, which ensures the feasibility of arbitrary pole placement for the third-order system.

3.2.2. Control law with integral action The control law for the augmented system (22) is defined as follows:

$$u = -K_a\, x_a, \tag{24}$$

where the augmented gain vector is

$$K_a = \begin{bmatrix} k_1 & k_2 & k_I \end{bmatrix}. \tag{25}$$

Expanding (24) in terms of the components of (25) yields

$$u = -k_1\, \eta - k_2\, \zeta - k_I\, x_I, \tag{26}$$

where k_1 and k_2 govern the dynamic response, while k_I determines the speed at which the steady-state error is eliminated. Thus, the closed-loop dynamics of the augmented system become:

$$\dot{x}_a = (A_a - B_a K_a)\, x_a. \tag{27}$$

3.2.3. Design by pole placement of the augmented system The design of K_a is carried out by pole placement on the pair (A_a, B_a), using the same specifications T_s and ξ from Section 3.1.2, with the natural frequency given by (15). Since the augmented system is of the third order, the specification of three poles is required. Two dominant poles are thus selected:

$$p_1 = -\xi\, \omega_n + j\, \omega_n \sqrt{1 - \xi^2}, \qquad p_2 = -\xi\, \omega_n - j\, \omega_n \sqrt{1 - \xi^2}. \tag{28}$$

A third real pole associated with the integrator dynamics is also selected:

$$p_3 = -\alpha\, \omega_n, \qquad \alpha \in [3,\, 10], \tag{29}$$

where α ensures that the integrator dynamics are sufficiently faster than those of the dominant poles, so that they do not significantly alter the specified transient response. The controller gains are obtained by applying Ackermann's formula to the augmented system:

$$K_a = \texttt{acker}(A_a,\, B_a,\, [p_1,\, p_2,\, p_3]). \tag{30}$$

4. Numerical validation

This section evaluates the performance of the controller applied to the second-order MLS model. For this analysis, the simulation parameters used in [28] were adopted, including the operating and current limits, the equivalent metallic mass, and the magnetic force constant. A detailed summary of these parameters is presented in Table 1.

Table 1. Parameters of the analyzed MLS

Parameter	**Value**	**Unit**
K_{mag}	2.4×10^{-06}	kgm/As^2
m	0.02985	kg
$y^\star$	20×10^{-03}	m
$i^\star$	0.9758	A
i_{min}	0	A
i_{max}	4	A

Three different positions were considered, and the mass was placed at different time intervals. In the first interval, between 0 and 2 seconds, the mass was positioned at $y^\star = 20$ mm. After 2-4 seconds, the reference changed to $y^\star = 24$ mm. Finally, the reference decreased to $y^\star = 16$ mm. For each control strategy, three case studies were considered, whose parameters are presented in Tables 2 and 3. Table 2 corresponds to the scenarios defined for the state-feedback control strategy introduced in Section 3.1 and evaluated in Section 4.1, whereas Table 3 corresponds to the scenarios associated with the state-feedback control with integral action.

Table 2. Scenarios evaluated for the design of the state feedback controller

Case	p_1	p_2	k_1	k_2
I	-40	-40	1600	80
II	-78	-37	2886	115
III	-20	-35	700	55

Table 3. Scenarios evaluated for the design of the integral action state feedback controller

Case	p_1	p_2	p_3	k_1	k_2	k_I
I	-20.5	-64	-42	4861	126	55104
II	-12	-35	-70	3710	117	29400
III	-60	-38.5	-29	5167	127	66990

To perform a quantitative performance comparison, each case was evaluated using different indices, including the integral of time multiplied by the absolute error (ITAE), the integral absolute error (IAE), the integral of time-weighted squared error (ITSE), the integral squared error (ISE), and the settling time t_s s [28]. These indicators allow analyzing the dynamic behavior of the system in terms of tracking error, thus providing an objective criterion to identify the control strategy with the best performance.

4.1. State feedback control

The state-feedback-based controller was designed by assigning the desired system poles, which are specified in (16). Once the desired poles had been established, they were used in the expression presented in (17), *i.e.*, the method for computing the controller gains using Ackermann's formulation. The values corresponding to the selected poles and the gains obtained for this control scheme are summarized in Table 2, which details the parameters used for the implementation of the controller in our case study. The corresponding responses for each control strategy are presented in Figure 2, where both the position and the current required by the actuator are shown. In addition, the numerical performance of the control metrics are presented in Table 4.

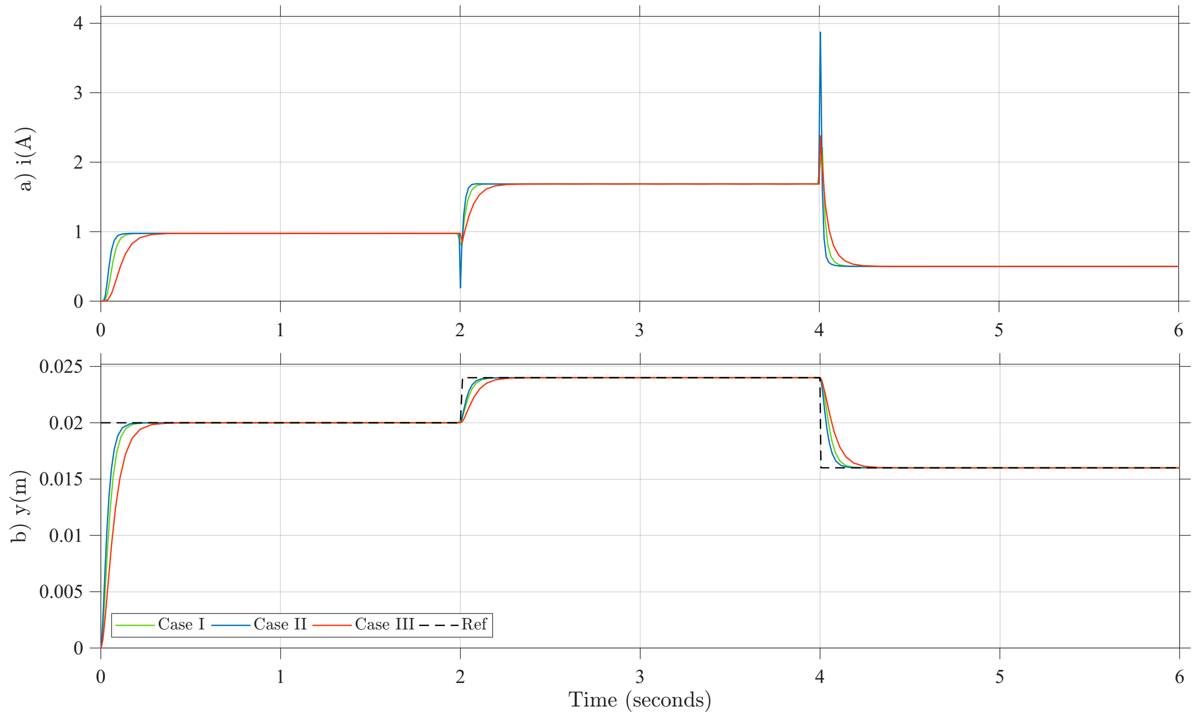

Figure 2. Levitator response to the state feedback control

Table 4. Summary of control indices evaluated via state feedback

Case	ITAE	IAE	ITSE	ISE	t_s[s]
I	0	1.6×10^{-3}	9.379×10^{-6}	1.501×10^{-5}	0.2219
II	4.084×10^{-6}	1.275×10^{-3}	7.203×10^{-6}	1.165×10^{-5}	0.1896
III	1.427×10^{-6}	2.514×10^{-3}	14.75×10^{-6}	2.322×10^{-5}	0.3591

Based on the behavior of the controller, which is depicted in Figure 2, and the numerical performance listed in Table 4, the following can be stated:

i. Among the three cases evaluated, important differences are observed regarding their performance indices. In the case of the ITAE, Case I reports a value equal to 0. However, this result is due to numerical rounding effects since the actual value is below the order of $\times 10^{-12}$. When comparing the other two cases, Case III exhibits a lower value (1.427×10^{-6}) than Case II (4.084×10^{-6}), which suggests a slightly faster and better-damped response for this specific index.

ii. As for the IAE, the lowest value corresponds to Case II (1.275×10^{-3}), when compared to the values for Cases I and III, respectively: 1.6×10^{-3} and 2.514×10^{-3}. This indicates that Case II exhibits reasonable damping and a better transient response.

iii. For the ITSE, Case II shows the best performance, with a value of 7.203×10^{-6}, approximately half of that recorded in Case III (14.75×10^{-6}) and lower than that obtained for Case I (9.379×10^{-6}). This result suggests that Case II is more effective in reducing larger-magnitude errors over time.

iv. In the ISE, Case II also exhibits the lowest value (1.165×10^{-5}), which indicates better performance in the initial instants. Although Case I reports a close value (1.501×10^{-5}), its behavior remains slightly inferior, while Case III shows the worst performance with 2.322×10^{-5}.

v. Finally, in terms of settling time, Case II reports the lowest value ($T_s = 0.1896$ s), compared to the $T_s = 0.2219$ s and $T_s = 0.3591$ s obtained for Cases I and III, respectively, which confirms a faster dynamic response of the system.

Based on these results, it can be concluded that Case II exhibits the best overall performance, as it achieves the most favorable values in four out of the five evaluation criteria.

4.2. *State feedback control with integral action*

The numerical performance of the state feedback controller that adds an integral action is reported in Figure 3 and Table 5.

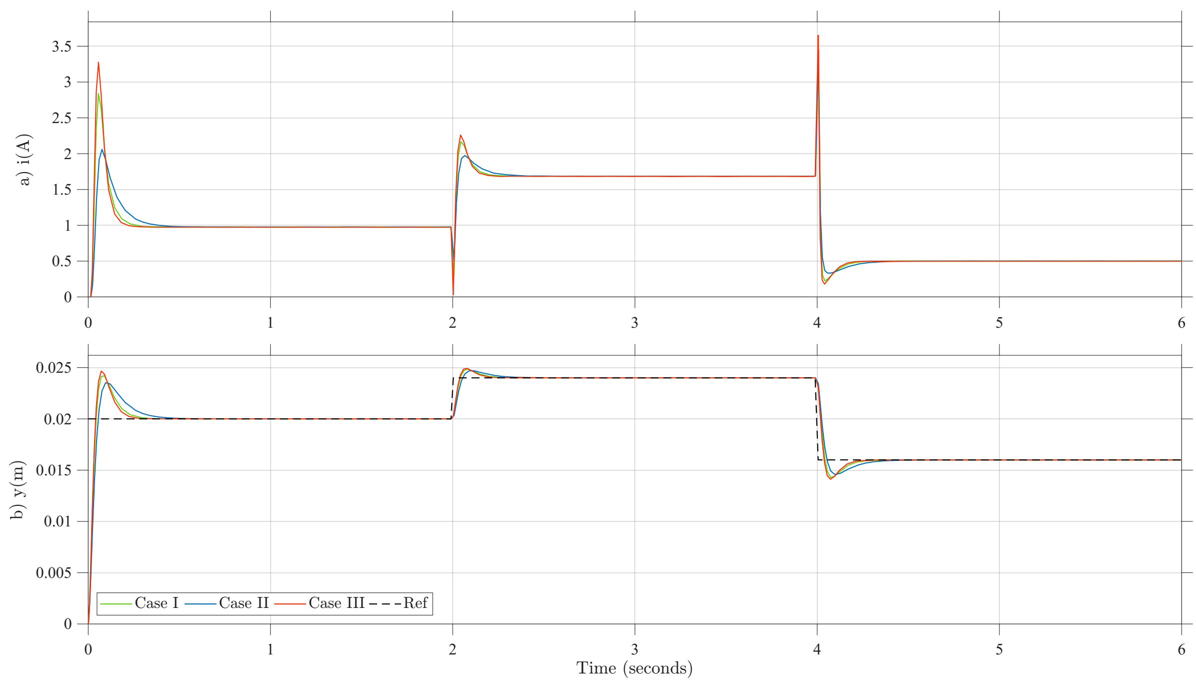

Figure 3. Levitator response to integral action state feedback control

Analogously to the analysis of the state feedback control, the evaluated cases for the controller including integral action are presented below:

i. In relation to the ITAE, Case II records the lowest value (0.539×10^{-5}). In contrast, Cases I and III exhibit higher values: 1.818×10^{-5} and 1.137×10^{-5}, respectively. This difference indicates that Case II provides better performance in terms of error reduction over time, which translates into a faster response with greater system damping.

Table 5. Summary of control indices evaluated by state feedback with integral action

Case	ITAE	IAE	ITSE	ISE	t_s[s]
I	1.818×10^{-5}	1.394×10^{-3}	5.593×10^{-6}	8.942×10^{-6}	0.3389
II	0.539×10^{-5}	1.685×10^{-3}	6.515×10^{-6}	10.32×10^{-6}	0.5044
III	1.137×10^{-5}	1.321×10^{-3}	5.432×10^{-6}	8.686×10^{-6}	0.3067

ii. Regarding the IAE, Case III achieves a better performance (1.321×10^{-3}), while Cases I and II show values of 1.394×10^{-3} and 1.685×10^{-3}. This result suggests that Case III provides a lower accumulation of absolute error, which is reflected in a more favorable transient behavior and an adequate level of damping.
iii. As for the ITSE, Case III exhibits the lowest value (5.432×10^{-6}), followed by Case I (5.593×10^{-6}) and Case II (6.515×10^{-6}). This comparison shows that Case III achieves a more efficient reduction of larger-magnitude errors over time, which translates into more favorable dynamic performance.
iv. In relation to the ISE, the lowest value corresponds to Case III (8.686×10^{-6}), indicating a better initial behavior. Case I reports a close value (8.942×10^{-6}), although slightly higher, while Case II records the highest value (10.32×10^{-6}), reflecting a less favorable performance according to this criterion.
v. In terms of settling times, Case III offers the best value ($T_s = 0.3067$ s), while Cases I and II reach times of 0.3389 s and 0.5044 s, respectively. These results show that Case III allows the system to reach the steady state in a shorter time interval, reflecting a faster dynamic response.

Based on the analysis of these indices, it can be determined that Case III exhibits the best overall performance, since it achieves the most favorable values in four out of the five evaluation criteria.

4.3. Comparison of results against a decoupled PI controller

The design of the PI controller proposed in [28] was developed based on a second-order model corresponding to a MLS. In a manner analogous to what is established in (8), the variable w is defined as the control input. In this case, the same criterion was adopted, considering an equivalent equilibrium point located at the origin of the coordinate system, which is defined as follows:

$$w = (\eta + y^{\star})^3 (\frac{m}{k_{mag}})(g - u), \tag{31}$$

where u represents an auxiliary control input employed for regulating the state variables. By substituting (31) into (6), the incremental model described in (9) and (10) is obtained once again.

When implemented in the decoupled system described in (9) and (10), the primary objective of the PI approach is the asymptotic stabilization of the system at the origin of the coordinate system. To this effect, the following PI controller structure is established:

$$u = -k_p \zeta - k_o \eta - k_i \int_0^t \zeta \, d\tau, \tag{32}$$

To evaluate the performance of the designed controller within a comparative framework, this section contrasts the best results obtained in the previous sections with the reference controller proposed in [28]. To this effect, a new naming convention for the evaluated cases is adopted. The case with the best performance in Section 4.1 (Case II) will hereafter be referred to as *Case II.I*. Similarly, the case with the best performance in Section 4.2 (Case III) will be denoted as *Case III.I*. Finally, the controller reported in [28], used as a reference for comparison, will be identified in this work as *Case I.I*. The numerical performance of this comparative analysis is depicted in Figure 4 and listed in Table 6.

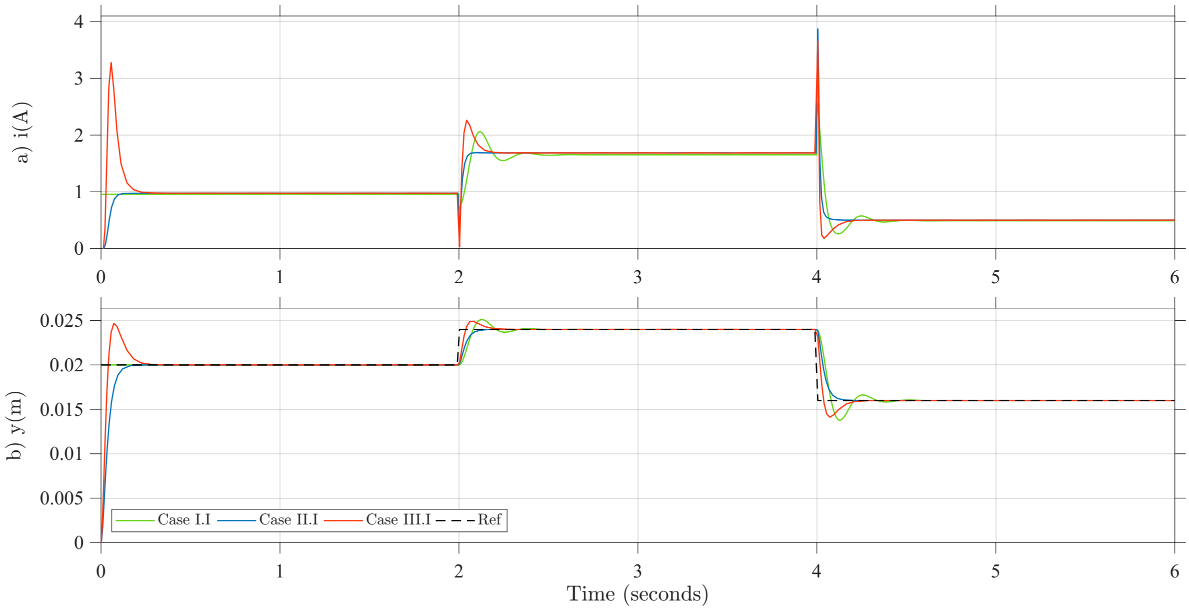

Figure 4. Comparison of the system's time response under three control strategies

Table 6. Summary of control indices *vs.* decoupled PI control

Case	ITAE	IAE	ITSE	ISE	t_s[s]
I.I	3.119×10^{-3}	1.058×10^{-3}	0.114×10^{-6}	3.143×10^{-6}	0.5
II.I	0.408×10^{-5}	1.275×10^{-3}	7.203×10^{-6}	1.165×10^{-6}	0.1896
III.I	1.137×10^{-5}	1.321×10^{-3}	5.432×10^{-6}	8.686×10^{-6}	0.3067

Based on the results presented in Table 6, the following can be stated:

i. In terms of the ITAE, Case II.I exhibits the lowest value (0.408×10^{-5}). Although Case III.I is slightly higher, by approximately 0.01 ms (1.137×10^{-5}), it still shows a better performance than Case I.I (3.119×10^{-3}), indicating that Case II.I has a greater ability to reduce errors that persist over time.
ii. Similarly, Case II.I achieves the lowest value regarding the ISE (1.165×10^{-6}), compared to 3.143×10^{-6} and 8.686×10^{-6} for Cases I.I and III.I, respectively, demonstrating a lower accumulated error energy throughout the process. Additionally, Case II.I records the shortest settling time ($t_s = 0.1896$ s).
iii. On the other hand, Case I.I reports the lowest values regarding the IAE (1.058×10^{-3}) and the ITSE (0.114×10^{-6}), which suggests a good performance in reducing absolute error and diminishing larger-magnitude errors. However, its settling time ($t_s = 0.5$ s) is significantly higher compared to the other analyzed cases.

Although Case I.I shows better performance in the IAE and ITSE, its settling time is considerably higher, which reflects a slower dynamic response and a delayed convergence to stability. Meanwhile, Case II.I offers the most balanced behavior regarding response speed and the reduction of accumulated error. This control case achieves the most favorable values in terms of the ITAE, the ISE, and settling times, demonstrating a greater ability to reduce persistent errors and reach the steady state in shorter periods of time.

4.4. Robustness analysis under measurement noise

To further deepen the analysis under conditions closer to reality, a noise signal was introduced into the measurement of the mass position, modeling disturbances associated with sensor noise and acquisition errors. This approach made it possible to evaluate the robustness of the previously designed controllers, specifically considering the most representative cases presented in Sections 4.1 and 4.2. Thus, the impact of noise on the dynamic performance of the system and the controllers' ability to maintain stability and tracking accuracy were analyzed.

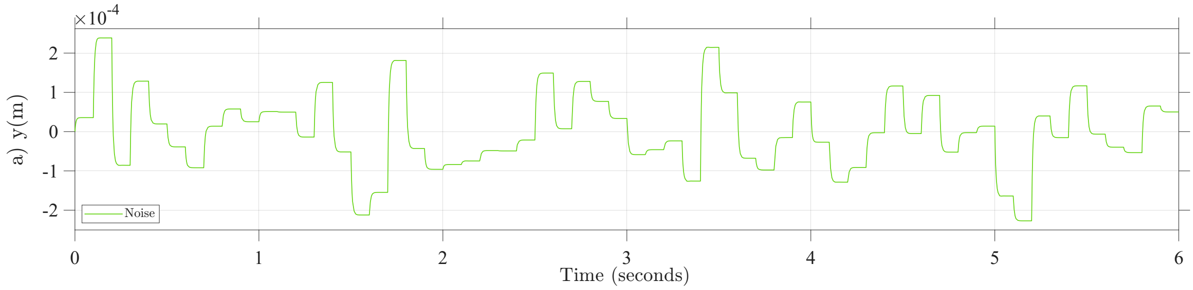

Figure 5. White noise applied to position measurement

The noise signal presented in Figure 5 corresponds to a white noise designed to emulate typical disturbances in measurement systems. Its magnitude allows representing a realistic scenario without introducing artificial instabilities, thereby facilitating the analysis of the system's behavior under random variations in the measurement.

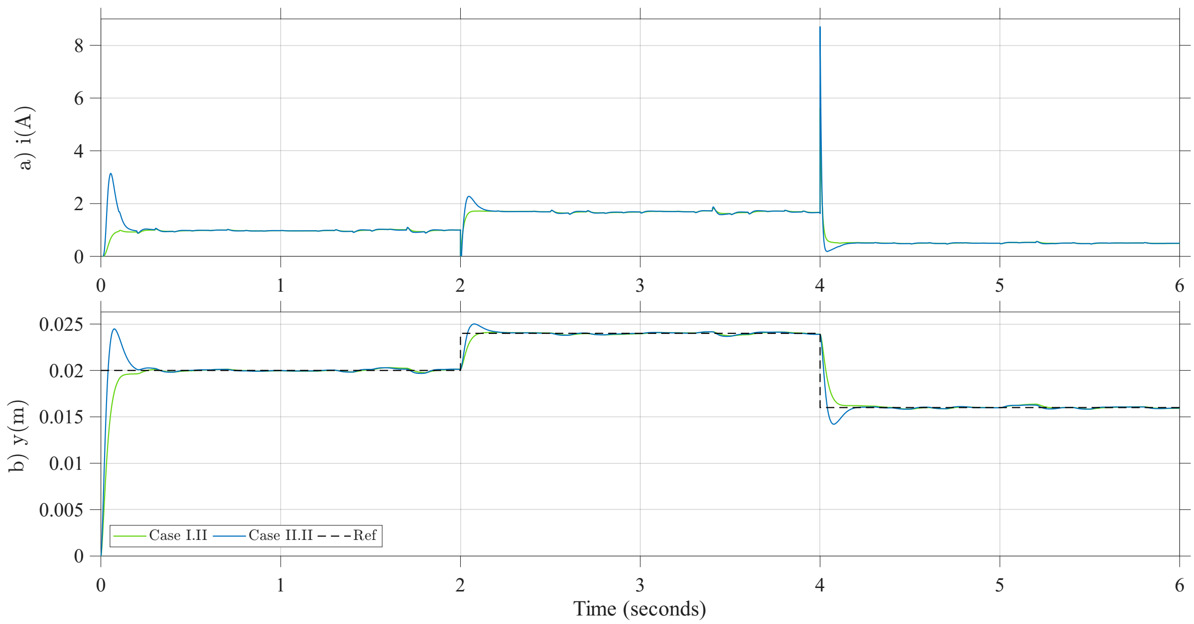

Figure 6. Comparison of the system's temporal response under noise regarding position measurement

Table 7. Summary of the control indices under noise regarding position measurement

Case	ITAE	IAE	ITSE	ISE	t_s[s]
I.II	0.199×10^{-3}	1.532×10^{-3}	7.073×10^{-6}	11.17×10^{-6}	0.255
II.II	6.481×10^{-6}	1.48×10^{-3}	5.306×10^{-6}	8.294×10^{-6}	0.334

Based on the results, significant differences between the evaluated cases are observed in terms of performance indices, as described in Table 7:

i. In particular, for the ITAE, Case II.II reports a value far below that of Case I.II. This difference—of several orders of magnitude—indicates that Case II.II has a greater ability to attenuate persistent errors over time, which translates into a more efficient response in terms of reference tracking.
ii. Regarding the IAE, Case II.II also achieves the lowest value compared to Case I.II. Although the difference is relatively small, this result indicates that Case II.II exhibits a lower accumulation of absolute error over time, reflecting a slightly more favorable transient response of the system.
iii. With respect to the ITSE, Case II.II again stands out, with the lowest value compared to Case I.II. This behavior suggests that Case II.II is more effective in reducing larger-magnitude errors over time.
iv. For the ISE, Case II.II maintains the best performance by recording the lowest value compared to Case I.II. This result demonstrates a lower total error energy, implying a more efficient system behavior in terms of accuracy.
v. Finally, regarding the settling time, Case I.II shows a better response compared to Case II.II. This indicates that Case I.II reaches the steady state in shorter time intervals, implying a faster response, albeit at the cost of higher accumulated error across the evaluated indices.

Based on this analysis, it can be concluded that Case II.II exhibits the best overall performance, as it achieves the most favorable values in the analyzed error indices. Although Case I.II stands out for its shorter settling time, Case II.II offers a more suitable trade-off between accuracy and dynamic performance. However, it should be highlighted that, given the system's limitations, these responses are not feasible in practice; around the fourth second, the actuator becomes saturated. Consequently, it is necessary to incorporate an additional filter to attenuate current spikes, preventing saturation and ensuring proper system operation.

5. Conclusions and future work

This article presented the design of a nonlinear controller for the stabilization of a MLS, which was modeled through an equivalent second-order linear representation. Two related control strategies were analyzed: the first based on state feedback and the second incorporating an additional integral action into this control structure, with the aim of improving reference tracking and stabilizing the metallic mass around the desired operating points. The results obtained from the simulations show that the placement of the closed-loop system poles has a direct influence on system dynamics. In particular, it was observed that certain pole configurations yield faster responses, albeit with a more oscillatory behavior, while other configurations produce more damped responses at the expense of longer settling times.

In the case of the state-feedback controller, the location of the first pole directly influences the system dynamics. In particular, placing it farther from the origin makes it possible to obtain faster responses. However, this improvement in response speed typically implies higher current consumption, given the larger control actions required to reach the reference point in shorter times.

The incorporation of integral action into the state-feedback controller helps to reduce the errors associated with significant changes in the system reference. This improves the tracking of the operating point and yields a more appropriate response to abrupt reference variations. However, this improvement in performance under disturbances or reference changes typically comes with a slight increase in settling time, on the order of a few milliseconds, compared to the state-feedback scheme without integral action.

When comparing the most representative cases of the state-feedback-based controllers and the decoupled PI control, it was observed that each strategy exhibits particular strengths with different degrees of suitability depending on application requirements. On one hand, state-feedback control allows for faster system responses, but this advantage usually implies higher current consumption. On the other hand, the decoupled PI controller shows a better performance in response to reference changes (as evaluated via the IAE and ITSE), favoring operating point tracking. Nevertheless, this strategy tends to exhibit a more oscillatory response compared to the state-feedback scheme.

When disturbances in the form of noise are incorporated into the system, additional differences in the performance of the evaluated control strategies become evident. Although a fast response is maintained, there is greater sensitivity to noise, which leads to increases in the control signal and the appearance of current spikes that may drive the system into saturation conditions.

These results highlight the importance of considering system robustness against external disturbances during the controller design stage. In this context, it becomes necessary to incorporate additional elements, such as filters in the control signal, to mitigate the effects of noise, reduce current spikes, and ensure that the system operates within its physical limits.

Future research should focus on experimentally validating the proposed scheme on a physical magnetic levitation platform to assess controller performance under real-world conditions, including measurement noise, actuator limitations, and unmodeled uncertainties. Subsequent work should evaluate controller sensitivity through deliberate parametric variations—such as changes in sphere mass or the magnetic constant—to quantify robustness and formally define stability margins. Additionally, optimization techniques like evolutionary algorithms or semidefinite programming could be explored for the automatic selection of pole locations in order to simultaneously optimize multiple performance indices. Finally, an additional filter could be incorporated into the control scheme to attenuate overshoots in response to abrupt reference changes, with the aim of achieving a faster response with a lower level of oscillation. It would be necessary to consider this filter in the presence of measurement noise, since it may generate peaks in the control signal that exceed the current limit, leading to system saturation.

ACKNOWLEDGEMENTS

The authors would like to thank the Curricular Project in Electrical Engineering for approving the undergraduate research titled *Diseño de controlador por realimentación de variables de estado para la estabilización de un levitador magnético considerando un modelo dinámico no lineal de segundo orden*. In addition, the authors acknowledge the assistance of the DeepSeek AI language model in refining the manuscript's language and structure. The tool was used solely for editorial purposes—such as rephrasing, grammar correction, and improving readability—whereas all technical formulations, methodological developments, numerical simulations, and scientific interpretations were conceived and executed by the authors.

Author's conflicts of interest

The authors declare no conflicts of interest.

Author's Contributions

O.D.M.: Conceptualization, formal analysis, investigation, writing, review, and editing.
C.A.V.-E.: Conceptualization, formal analysis, assembly, investigation, methodology, simulation, original draft writing, and review.
J.S.S.-R: Conceptualization, formal analysis, investigation, assembly, methodology, simulation, original draft writing, and review.

REFERENCES

1. Muhammad Adnan, Baohua Xiao, Muhammad Ubaid Ali, Shaheen Bibi, Hong Yu, Peiwen Xiao, Peng Zhao, Haiyan Wang, and Xianjin An. Human inventions and its environmental challenges, especially artificial intelligence: New challenges require new thinking. *Environmental Challenges*, 16:100976, August 2024.
2. Nikolay Hinov. From Energy Efficiency to Energy Intelligence: Power Electronics as the Cognitive Layer of the Energy Transition. *Electronics*, 14(23):4673, November 2025.
3. Ogata and Katsuhiko. *Ingenieria de Control Moderna*. Prentice-Hall Hispanoamericana, Mexico, 3 edition, 2010.
4. Pablo Andrés Muñoz Gutiérrez, Eduardo Giraldo Suárez, and Jhon Abraham Bonilla Becerra. Identificación y control de un Vehículo Aéreo no Tripulado tipo Quadcopter. *Ingenierías USBMed*, 7(1):5–10, June 2016.
5. Oscar Danilo Montoya Giraldo, Walter Gil-González, and Adolfo Jaramillo-Matta. A generalized backstepping controller design for a second-order magnetic levitation system. *Statistics, Optimization & Information Computing*, 13(1):286–296, October 2024.
6. Teschl and Gerald. *Ordinary Differential Equations*. American Mathematical Society, 2012.

7. Abdullah Mughees and Syed Ali Mohsin. Design and Control of Magnetic Levitation System by Optimizing Fractional Order PID Controller Using Ant Colony Optimization Algorithm. *IEEE Access*, 8:116704–116723, 2020.
8. Dini Wang, Fanwei Meng, and Shengya Meng. Linearization Method of Nonlinear Magnetic Levitation System. *Mathematical Problems in Engineering*, 2020:1–5, June 2020.
9. Maher Alwajih and Shabana Urooj. *Characterization and Control Strategies of a Magnetic Levitation System*, pages 175–182. Springer Singapore, October 2017.
10. A. Bilal Ozcan, Ismail Bayezit, and Mert Tekyurt. Stabilization of Chaotic Systems using Hardware-in-the-Loop Validation for Sliding Mode Control and Input State Linearization. *The Journal of Engineering*, 2025(1), January 2025.
11. Štefan Chamraz, Mikuláš Huba, and Katarína Žáková. Stabilization of the Magnetic Levitation System. *Applied Sciences*, 11(21):10369, November 2021.
12. Edwin René Aguilar-Jaramillo and Víctor Gonzalo Proaño Rosero. Aplicación de las LMI al diseño de controladores robustos. *Ingenius*, (18):93, July 2017.
13. Maria Hypiusova and Alena Kozakova. Robust PID controller design for the magnetic levitation system: Frequency domain approach. In *2017 21st International Conference on Process Control (PC)*, pages 274–279. IEEE, June 2017.
14. Jonathan Smith Castro Beltrán, Carlos Felipe Vergara Ramírez, and Joan Stiven Herrera Guayazan. Comparación de un control lineal y no lineal en un levitador magnético. *Ingenierías USBMed*, 9(1):112–118, February 2018.
15. Yair Lozano Hernández, Oscar Octavio Gutiérrez Frías, and Mario Villafuerte Bante. Control pi difuso de un sistema de levitación magnética mediante un sistema embebido. *Ingeniería Investigación y Tecnología*, 20(4):1–11, October 2019.
16. Lei Zhou and Jingjie Wu. Magnetic Levitation Technology for Precision Motion Systems: A Review and Future Perspectives. *International Journal of Automation Technology*, 16(4):386–402, July 2022.
17. Qi Zhu, Su-Mei Wang, and Yi-Qing Ni. A Review of Levitation Control Methods for Low- and Medium-Speed Maglev Systems. *Buildings*, 14(3):837, March 2024.
18. Shekhar Yadav, S.K. Verma, and S.K. Nagar. Optimized PID Controller for Magnetic Levitation System. *IFAC-PapersOnLine*, 49(1):778–782, 2016.
19. Sandra Milena Zambrano and Anderson Vera Correa. Design of a system of control for feedback from the balances of matter and energy for the evaporator double effect of the laboratory of chemical engineering of the university of pamplon. *Infométrica*, 2:125–148, 2019.
20. Guancheng Liu, Yonghua Lu, Jiajun Xu, Zhanxiang Cui, and Haibo Yang. Magnetic Levitation Actuation and Motion Control System with Active Levitation Mode Based on Force Imbalance. *Applied Sciences*, 13(2):740, January 2023.
21. Ziyang Hao, Linjie Hao, Pengfei Liu, Ruichen Wang, and Meiqi Wang. Research on Levitation Control of a Two-Degree-of-Freedom System Based on IWOA-ISMC. *Actuators*, 15(2):118, February 2026.
22. Marlon Cruz-Pegueros, Oscar Octavio Gutiérrez Frías, Norma Beatriz Lozada-Castillo, and Alberto Luviano-Juárez. Modelado y control de un sistema de levitación magnética basado en un cojinete magnético activo. *Nova Scientia*, 9(19):229, September 2017.
23. Francesco Ferrante, Chiara Ravazzi, and Fabrizio Dabbene. An lmi approach for structured h_∞ state feedback control∗∗the authors' research has been partially supported by the prin 2017 project, prot. 2017s559bb. *IFAC-PapersOnLine*, 53(2):4058–4063, 2020. 21st IFAC World Congress.
24. Rene Alexander Palacios Ochoa. Controlador con Observador de Estados de Orden Completo para un motor de DC mediante dSPACE. *MASKAY*, 7(1):6, October 2017.
25. Oscar H Sierra-Herrera, Luis D Patarroyo-Gutiérrez, and Mario E González-Niño. Simulation-based comparison of ADRC, PI, and PID controllers on a SEPIC converter: performance and complexity. *Ingeniería y Competitividad*, 27(3), November 2025.
26. Aichen Wu, Xipeng Wu, Fazhi Song, Pengyu Sun, and Jiubin Tan. A pole-placement-based variable-gain observer for precision motion stages: Addressing the disturbance-noise trade-off. *Actuators*, 15(2), 2026.
27. Mundher H.A. Yaseen and Haider J. Abd. Modeling and control for a magnetic levitation system based on simlab platform in real time. *Results in Physics*, 8:153–159, March 2018.
28. Oscar Danilo Montoya Giraldo, Walter Julián Gil-González, and Andrés Leonardo Jutinico-Alarcón. A Decoupled PI Design for a Second-Order Model of a Magnetic Levitation System. *Statistics, Optimization & Information Computing*, 14(2):628–635, May 2025.
29. Ricardo Lopes Coelho. Newton's second law and physics textbooks. *Foundations of Science*, 31:179–204, July 2025.
30. Mundher H.A. Yaseen and Haider J. Abd. Modeling and control for a magnetic levitation system based on SIMLAB platform in real time. *Results in Physics*, 8:153–159, March 2018.
31. Dillip Kumar Mishra, Mohammad Hossein Abbasi, Mohsen Eskandari, Saroj Paudel, Sourav K. Sahu, Jiangfeng Zhang, and Li Li. State–space modelling and stability analysis of solid-state transformers for resilient distribution systems. *Applied Sciences*, 14(5), 2024.
32. Danica Rosinova, Richard Schwarz, and Alena Kozakova. Air levitation state feedback control using pole placement and kalman filter. *IFAC-PapersOnLine*, 58(25):132–137, 2024.
33. Richard Seeber and Markus Tranninger. Integral state-feedback control of linear time-varying systems: A performance preserving approach. *Automatica*, 136, 2022.
34. Hong Jiang, Guangren Duan, and Mingzhe Hou. Generalized proportional–integral extended state observer-based controller design for fully actuated systems. *ISA Transactions*, 155:137–147, 2024.
35. Sohaibullah Zarghoon and Cyril Belavý. Lqr and pole placement controllers with integral action design technique and performance analysis for control of temperature field in continuous casting process. In *2023 24th International Carpathian Control Conference (ICCC)*, pages 489–494. IEEE, 2023.
36. Gopal Jee and Santanu Dasgupta. Generalization of ackermann's formula for state-feedback of multi-input systems. *IFAC-PapersOnLine*, 57:196–201, 2024.